Superdiffusive transport by multivalent molecular walkers moving under load

Mark J. Olah and Darko Stefanovic

Phys. Rev. E **87**, 062713 — Published 24 June 2013

DOI: 10.1103/PhysRevE.87.062713

Superdiffusive transport by multivalent molecular walkers moving under load

Mark J. Olah* and Darko Stefanovic†
Department of Computer Science, University of New Mexico,
MSC01 1130, 1 University of New Mexico, Albuquerque, NM 87131-0001

We introduce a model for translational molecular motors to demonstrate that a multivalent catalytic walker with flexible, uncoordinated legs can transform the free energy of surface-bound substrate sites into mechanical work and undergo biased, superdiffusive motion, even in opposition to an external load force. The walker in the model lacks any inherent orientation of body or track, and its legs have no chemomechanical coupling other than the passive constraint imposed by their connection to a common body. Yet, under appropriate kinetic conditions the walker's motion is biased in the direction of unvisited sites, which allows the walker to move nearly ballistically away from the origin as long as a local supply of unmodified substrate sites is available. The multivalent random walker model is mathematically formulated as a continuous-time Markov process and is studied numerically. We use Monte Carlo simulations to generate ensemble estimates of the mean squared displacement and mean work done for this non-ergodic system. Our results show that a residence time bias between visited and unvisited sites leads to superdiffusive motion over significant times and distances. This mechanism can be used to adapt any enzyme–substrate system with appropriate kinetics for use as a functional chemical implementation of a molecular motor, without the need for structural anisotropy or conformationally mediated chemomechanical coordination.

Keywords: molecular motors, molecular walkers, kinetic Monte Carlo, Metropolis-Hastings, superdiffusive motion

I. INTRODUCTION

Motion at the nanoscale is dominated by random, thermally driven collisions that lead to slow, uncontrollable *diffusive transport*. Diffusion of large cargo molecules in a crowded cellular environment is so slow that nature has evolved sophisticated, specialized molecular machines to transport cargo directionally at superdiffusive rates. These translational molecular motors, such as kinesin, dynein, and myosin [1], walk along *oriented* tracks, consuming chemical energy in the form of ATP and converting it to mechanical energy that is used to do work against external load forces [2, 3]. Molecular motors are essential to a cell's ability to control the distribution and movement of materials and information within it.

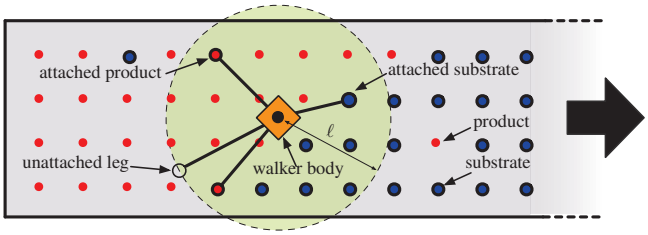

FIG. 1: (color online) A multivalent random walker (MVRW) is an abstract model of a multivalent enzyme with a rigid, symmetric body and k identical enzymatic legs that can reversibly attach to surface-bound chemical sites. Each leg is flexibly-tethered to the body with maximum extension length ℓ. The enzymatic action of a leg can irreversibly transform a substrate site into a product, changing the subsequent binding kinetics for the site. As the legs attach to and detach from sites, the walker moves over the surface.

Synthetic nanoscale systems, like the natural cellular systems that have inspired their development, also need mechanisms to maintain non-equilibrium distribution of materials and information [4]. Useful synthetic behavior has been demonstrated by combining natural molecular motors and components in novel ways [5]. However, each species of natural molecular motor is highly specialized to its cellular environment, chemical fuel source, and polymeric track (e.g., microtubules, actin, or DNA). Synthetic systems with different polymers must either adapt existing natural motors, or use newly designed compatible synthetic motors. Kinesin and other natural motors can be mutated to change the kinetics of their motion [6], but not to catalyze arbitrary fuel substrates, or move over arbitrary tracks without fundamentally altering their functionality or efficiency. Natural molecular motors rely on non-local conformational changes to couple the binding of fuel with the kinetics of track binding [7], and use this conformationally-mediated chemomechanical coupling to coordinate their processive hand-over-hand walking gait [8]. These mechanisms make natural motors efficient but also hard to mimic in synthetic systems.

We show that neither oriented tracks, nor rigid walking gaits, nor chemomechanical coupling, nor coordinated conformational changes, are necessary for a molecular walker to do ordered mechanical work as a molecular motor.[1] We consider the motion of a multivalent walker with a rigid, inert body and several flexible, enzymatic legs (Fig. 1). The legs attach to and enzymatically modify surface-bound chemical sites arrayed as

*Electronic address: mjo@cs.unm.edu
†Electronic address: darko@cs.unm.edu; to whom correspondence should be sent

[1] As described below, our model can be compared with much simpler models of multivalent enzymatic walkers as proposed by Antal and Krapivsky [12, 13]. While the ability to act as a motor is immanent to multivalent enzymatic walkers, the simpler models lack the representational detail needed to quantify the ability of walkers to perform physical work. Below we elaborate on other functional distinctions between the models.

arbitrary 2D patterns and tracks. The legs are chemically and conformationally uncoupled, other than by the passive constraint imposed by the connection to a common body. Yet, under appropriate kinetic conditions, the walker can be made to move directionally and processively even in opposition to a force. By modeling and understanding such simple walker systems, we learn which chemical and mechanical properties of walker-based motors are sufficient for superdiffusive motion, and which properties are not necessary.

Our multivalent random walker (MVRW) model is an abstract description of the motion of these walkers. It takes the form of a continuous time Markov process that describes the stochastic motion of a walker as it moves over and modifies surface-bound sites. The model is designed so that the Markov process can be efficiently simulated, yet still accurately model the effect of external forces on the physical motion and chemical action of the walker's body and legs.

Through Monte Carlo simulations we show that walkers with appropriate kinetics can move superdiffusively in the direction of unvisited sites over significant times and distances, and can do so while performing a non-trivial amount of work against an external load. This effect can be understood from the spontaneous emergence of a substrate concentration gradient—a boundary between visited product sites and unvisited substrate sites. At this boundary, the non-uniform local substrate concentration combined with the chemical kinetics of the legs and the constraints that the body places on leg motion lead to a directional bias away from previously visited sites. As the legs irreversibly modify substrates to products, they move this bias-inducing boundary further from the origin. Hence, as long as a walker stays proximate to the boundary it moves ballistically away from the origin.

The MVRW model is inspired by attempts to model the motion of synthetic DNA-based molecular walkers, called *molecular spiders* [9], and a desire to aid in the design of new laboratory experiments involving molecular spiders. The spiders are structurally similar to the abstract walker shown in Fig. 1. Chemically, molecular spiders employ a deoxyribozyme–oligonucleotide [10] enzyme–substrate system, where the deoxyribozyme legs can bind to and modify (cleave) the oligonucleotide substrates attached to the surface. Molecular spiders have been observed to walk processively in 3D environments [9], and move directionally over 2D nanoscale tracks [11]. Abstract models of 1D spider motion were first proposed by Antal and Krapivsky [12, 13], who showed that spiders with rigid nearest-neighbor hopping gaits and idealized kinetics would experience an effective bias towards unvisited sites. Subsequent simulations [14] have shown this *AK spider model* to exhibit transient superdiffusive behavior as the walkers move between periods of ballistic and diffusive motion depending on the walker's position with respect to the boundary between visited and unvisited sites. Other work has extended the AK model to study mathematical properties of AK spider walks in 1D [15–17] and 2D [18]; the collective and cooperative behavior of multi-spider systems in 1D [19–21]; and the effect of a load force on the rigid 1D walking gaits of AK-like spiders under the kinetic rates specific to deoxyribozymes [22, 23].

However, it remains unclear how the rigid 1D gaits of the AK model and its derivatives can be implemented at the chemical level. Indeed, sophisticated mechanisms are necessary for the coordinated stepping of the natural cytoskelatal motors like kinesin I and myosin V, which rely on oriented tracks, conformational switching, and long-range chemomechanical coordination to achieve directed, hand-over-hand walking gaits [24, 25]. Deoxyribozyme-based molecular spiders lack these structural features, and there is no evidence to show that coordinated hand-over-hand, inchworm, or nearest-neighbor stepping gaits can be realized directly by molecular spiders. The MVRW model removes any assumptions of leg coordination, and places no constraints on the gaits of the walker legs, other than the passive constraint imposed by the finite length of legs and their connection to a common body. This is achieved by considering a more sophisticated model of the mechanical equilibrium of the walker body and unattached legs which allows the effect of a load force on the body motion and the leg attachment rates to be efficiently simulated. Yet the MVRW model still imposes inherently simple structural requirements on the walkers it models which do not require any sophisticated coordination between the legs, making the model generally applicable to *any* enzyme–substrate walker system that shares the simple structural motif of a rigid, inert body with flexibly tethered enzymatic legs like the walker in Fig. 1. Hence, the MVRW model is not an extension of the Antal-Krapivsky spider models, in the sense that the AK model is not a special case of the MVRW model. Nor is the MVRW model a direct model of deoxyribozyme-based molecular spiders, as it remains abstract enough to serve as a general model of uncoordinated, unoriented, enzymatic walkers. This abstraction allows us to show that such a structurally simple walker design, using any enzyme–substrate system with appropriate kinetics, can be made to move superdiffusively even under the direct application of a load force to the body, transforming the chemical free energy of substrate sites into physical work.

The simulation results and analysis of the MVRW model we present show that mechanisms for designing molecular motors exist without the need for chemomechanical coupling, conformational coordination, rigid walking gaits, or inherent orientation of walker and track. Multivalent random walkers, like natural molecular motors, are Brownian ratchets [26] that rectify random molecular motion into ordered work and directional transport. Both systems achieve this rectification by utilizing the chemical free energy of a substrate fuel. However, the mechanisms by which MVRWs do this are significantly different from natural motors. Unlike kinesin I, myosin V, and other natural cytoskelatal motors, multivalent random walkers move over arbitrarily arranged 2D tracks, and are able to do so without inherent orientation or structural asymmetry. The gaits of a multivalent random walker are uncoordinated and acyclic, yet the irreversible modification of surface sites causes an emergent asymmetry in local substrate concentrations that is able to bias the motion of walkers, allowing them to move directionally along prescriptive landscapes. The structural and chemical simplicity of MVRWs is one of their most important properties as it means that the conceptual

functionality of a molecular spider is independent of the specific enzyme–substrate system used in their implementation. Hence, multivalent random walkers provide a different perspective for better understanding what structures, properties, and mechanisms are minimally necessary to turn a molecular walker into a molecular motor.

II. THE MULTIVALENT RANDOM WALKER MODEL

We model the motion of a multivalent random walker as a continuous-time, discrete-state Markov process, where each state transition corresponds to a chemical reaction between a leg and a surface-bound site. The model conceptually separates the timescales of the relatively slow leg–site interactions from the much faster physical (mechanical) motion of the walker's body and legs. In this way, only chemical reactions correspond to state transitions in the Markov process, and the state space remains discrete. The Markov property is ensured by assuming that the physical motion of the position of the body and unattached legs comes to an equilibrium in between successive chemical reactions.

The MVRW model is 2D and consists of a walker and an environment of surface-bound sites. The walker has a rigid, point-like body which serves as the attachment point for k flexibly tethered legs, each with maximum length ℓ. The environment is described by a set $\mathbf{S} \subset \mathbb{R}^2$ of immobile chemical sites. All sites are initially substrates, but they can be transformed into products by the enzymatic action of a leg.

The state of the Markov process needs only to describe the state of the *reactive* chemicals in the system, i.e., the species at each chemical site and the chemical state of each leg. The state of the surface is defined by the set P of sites that have been transformed to products; all other sites in $\mathbf{S}$ are considered to be substrates. A walker leg is either attached to a site in $\mathbf{S}$ or is detached. No two legs may be attached to the same site. The state of the walker is succinctly represented by the set $A \subset \mathbf{S}$ of attached sites, where $0 \leq |A| \leq k$. Thus, any state ω can be described compactly as $\omega = (P,A)$, and we let Ω be the set of all potential states.

A. Chemical kinetics and state transitions

In the MVRW model we assume each leg has a single enzymatic site that can bind to and irreversibly modify a substrate site into product. The kinetics of an enzymatic leg (L) binding to substrate (S) and product (P) sites can be described by five reaction rates

$$\begin{aligned} \mathrm{L} + \mathrm{S} &\underset{k_\mathrm{S}^-}{\overset{k_\mathrm{S}^+}{\rightleftarrows}} \mathrm{LS} \xrightarrow{k_\mathrm{cat}} \mathrm{L} + \mathrm{P} + \mathrm{P}^* \\ \mathrm{L} + \mathrm{P} &\underset{k_\mathrm{P}^-}{\overset{k_\mathrm{P}^+}{\rightleftarrows}} \mathrm{LP} \end{aligned} \tag{1}$$

In Eq. 1, we define the k_cat reaction to encompass both the actual catalytic cleavage of the LS complex together with the subsequent dissociation of leg L from the surface-bound product P, and any other auxiliary product P^*. We assume the auxiliary (waste) product P^* is not bound to the surface and its bulk concentration in solution, $[\mathrm{P}^*]$, is essentially 0. Thus, individual rates of binding and unbinding of P^* are not important, and the dissociation reactions can be rolled into the rate k_cat. The assumption of irreversibility holds when the Gibbs free energy, ΔG, of the catalysis reaction is strongly negative, and the rate of the reverse pathway is effectively zero, which would be the case if $[\mathrm{P}^*] \approx 0$.

The advantage of this definition of k_cat is that there is a direct correspondence from reaction rates to Markov process transitions. The reactions of Eq. 1 each correspond to one of three types of functional motion for walker legs, association (binding), dissociation (unbinding), and catalysis. Each of these actions corresponds directly to a transition in the walker Markov process. In the MVRW model, we assume that rates for the unimolecular dissociation and catalysis reactions for a leg–site complex are not chemomechanically coupled to the conformations or positions of the body and other legs. Thus, as in the unimolecular stochastic kinetic models of Gillespie [27], each individual LS or LP complex will dissociate or undergo catalysis according to the rates k_S^-, k_P^-, and k_cat, and the time until that reaction happens will be exponentially distributed according to the sum of the potential reaction rates from that bound state.

The bimolecular association reactions are more complicated to model as their propensity depends not only on rates k_S^+ and k_P^+, but also on the likelihood of the leg being proximate to the chemical site in order that it may bind. This likelihood, in turn, depends on the position of the body and the unattached legs.

B. The body's equilibrium position

Molecular motors and molecular walkers operate in a regime where they are almost always at physical (mechanical) equilibrium with their surroundings [28], and this fact is critical to understanding how molecular motors operate at the level of discrete chemical transitions [29–31]. After each chemical reaction of a leg attaching, detaching, or cleaving, the walker's body is subject to high-frequency thermally-driven constrained diffusion, which quickly brings the walker body to a physical (mechanical) equilibrium distribution $\mathbf{B}$ over 2D positions on the surface. This ensures that the Markov property holds for the discrete chemical states in the MVRW stochastic process because the high-frequency physical motion of the walker quickly removes any conformational memory of previous chemical states, and the body distribution $\mathbf{B}$ only depends on the current state $\omega = (P,A)$, and not on any previous states in the Markov process.

We assume that the only coupling between the attached legs and the body is that the body is constrained to stay within distance ℓ from each attached site. Hence, $\mathbf{P}[\mathbf{B} = \mathbf{p}] = 0$ for position $\mathbf{p} \in \mathbb{R}^2$ if there is any attached leg site $\mathbf{s} \in A$ such that $\|\mathbf{p} - \mathbf{s}\| > \ell$. We call all values of $\mathbf{p}$ that satisfy $\|\mathbf{p} - \mathbf{s}\| \leq \ell$ for all $\mathbf{s} \in A$ the *feasible body positions*, $\mathcal{F}$, illustrated in Fig. 2.

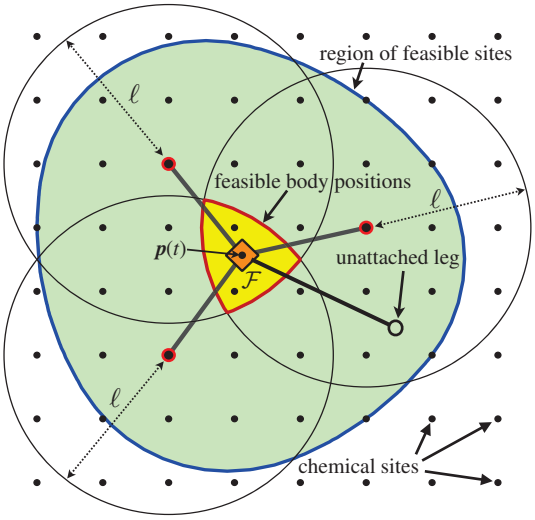

FIG. 2: (color online) The feasible body positions, $\mathcal{F}$, as determined by the attached leg constraints are labeled and shown in yellow. Any site at most distance ℓ from $\mathcal{F}$ is a feasible site (labeled and shown in green).

At equilibrium, $\mathbf{B}$ is a Boltzmann distribution over the feasible positions $\mathbf{p} \in \mathcal{F}$ according to the energy $U(\mathbf{p})$ at each position,

$$\mathbf{P}[\mathbf{B} = \mathbf{p}] = p_{\mathbf{B}}(\mathbf{p}) = \frac{e^{-\beta U(\mathbf{p})}}{\int_{\mathcal{F}} e^{-\beta U(\mathbf{p})} d\mathbf{p}}. \tag{2}$$

In Eq. 2, $\beta = 1/k_B T$, where k_B is Boltzmann's constant and T is absolute temperature. The energy $U(\mathbf{p})$ necessarily depends on the entropic and mechanical properties of the walker legs and their tethers, the details of which are possible to model in $U(\mathbf{p})$, but are dependent on the actual chemical construction of the walker legs and tethers. To keep our analysis generally applicable to any flexible tether, we choose a null hypothesis of no mechanical coupling or internal structure to the legs, and model the energy $U(\mathbf{p})$ as uniform over any feasible position, but infinite for infeasible positions,

$$U(\mathbf{p}) = \begin{cases} 0 & \mathbf{p} \in \mathcal{F} \\ \infty & \text{otherwise} \end{cases}. \tag{3}$$

C. Leg–site binding kinetics

The bimolecular kinetics of leg–site binding is controlled by two factors, (I) a second-order process by which the leg and site come into contact, and (II) a first-order process wherein the leg and site undergo conformational changes to move to a strongly bound state [28]. We consider the case when the legs are short enough, and the conformational changes leading to binding are slow enough that factor II is limiting. In this case, an unattached leg undergoing constrained diffusion has the opportunity to interact many times with the local feasible sites before it finally binds strongly enough to be considered attached. The overall rate of a leg reacting with any feasible site is then proportional to the number of feasible sites in its proximity. Equivalently, from the perspective of a feasible site, the probability that it reacts with the leg is independent of the number of other feasible sites in the local environment. For any site $\mathbf{s}$ and body position $\mathbf{b}$ we define a feasibility function,

$$f_{\mathbf{s}}(\mathbf{b}) = \begin{cases} 1 & \|\mathbf{s} - \mathbf{b}\| < \ell \\ 0 & \text{otherwise} \end{cases}. \tag{4}$$

Then from position $\mathbf{b}$, an unattached leg binds to site $\mathbf{s}$, with species $\pi(\mathbf{s}) \in \{\mathrm{S}, \mathrm{P}\}$, with rate

$$r_{\mathbf{b}}(\mathbf{s}) = k^{+}_{\pi(\mathbf{s})} f_{\mathbf{s}}(\mathbf{b}). \tag{5}$$

Now, we take into account that the body is not at a single position $\mathbf{b}$, but in an equilibrium distribution $\mathbf{B}$ over positions, and we integrate Eq. 5 to obtain

$$r_{\mathbf{B}}(\mathbf{s}) = k^{+}_{\pi(\mathbf{s})} \int_{\mathcal{F}} p_{\mathbf{B}}(\mathbf{b}) f_{\mathbf{s}}(\mathbf{b})\, d\mathbf{b}. \tag{6}$$

Any site with non-zero rate of attachment is called a *feasible site*; the region of feasible sites is shown in Fig. 2.

D. The effect of force on walkers

The MVRW model can also capture the effect of forces on the walker body. This is an advantage of modeling the body's position as a Boltzmann distribution determined by the energy of the walker at each feasible position. Under the effect of a conservative load force $\mathbf{f}$, the energy of position $\mathbf{p}$ is

$$U_{\mathbf{f}}(\mathbf{p}) = U(\mathbf{p}) - \mathbf{f} \cdot (\mathbf{p} - \mathbf{p}_0), \tag{7}$$

where $\mathbf{p}_0$ can be any reference point. The energy $U(\mathbf{p})$ is the energy of the body at position $\mathbf{p}$ under zero force, which is defined in Eq. 3 using our assumption of a uniform $U(\mathbf{p})$. This choice of $U(\mathbf{p})$ represents a worst-case scenario from the perspective of force production by walkers, as the mechanical structure of the attached legs is not able to oppose any forces acting on the walker. Despite this disadvantage, we will show in Sec. IV that walkers can still move superdiffusively in opposition to a load force applied to the body.

The adjusted energy $U_{\mathbf{f}}$ in Eq. 7 gives a new equilibrium distribution with probability mass shifted in the direction of the applied force. The effect of force on the body's equilibrium position and on the attachment propensity for each of the feasible sites is illustrated in Fig. 3.

III. SIMULATION AND ANALYSIS METHODS

The MVRW model is a continuous-time Markov process (CTMP) with discrete states $\omega = (P, A) \in \Omega$. Given all relevant parameters, the walker CTMP defines certain random variables $\{X(t)\}_{t \geq 0}$ over the state space Ω. This single Markov process simultaneously describes the fast physical motion of the walker body and legs under an external

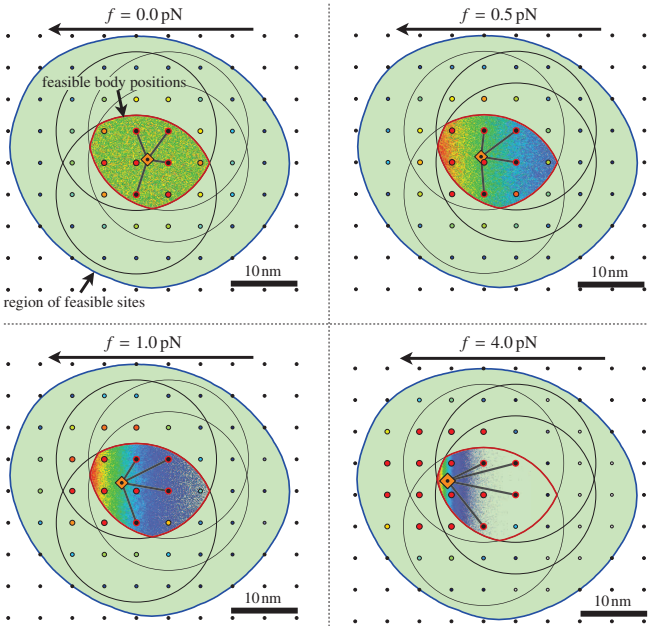

FIG. 3: (color online) The equilibrium body position probability density for a walker under several different load forces. Warmer colors represent increasing probability. The body is drawn at its mean equilibrium position, $\langle \mathbf{B} \rangle$. The region of feasible sites is labeled and illustrated in green, but not all sites are equally likely for attachment. The color and size of feasible sites indicate the effective attachment rate as determined by the body position distribution **B**.

load, as well as the slower discrete chemical state changes of the legs binding and modifying the surface sites. The MVRW simulation process uses a kinetic Monte Carlo algorithm [32, 33] to sample from the *non-equilibrium* behavior of the walker's *chemical* motion, but each chemical step in this MVRW Markov Chain requires using the Metropolis-Hastings algorithm to sample the *equilibrium* behavior of the body's *physical* motion. Hence, by separating the timescales of the chemical from the physical behavior of the system, we can take advantage of both equilibrium and non-equilibrium Markov chain Monte Carlo techniques, using each technique where it is most applicable to the dynamics of the walkers.

Our kinetic Monte Carlo (KMC) algorithm for the MVRW process produces samples $x(t)$ for $t \in [0, t_{\max}]$, such that at each time, $x(t)$ is a sample of a random variable $X(t)$. With an ensemble of n samples of the Markov process, we measure and report various properties of the system state at linearly and logarithmically spaced time points $t \in [0, t_{\max}]$. The simulation algorithm is described in detail in previous work [34, 35].

In order to compute the transition rates for the association reactions, we use the Metropolis-Hastings algorithm [36–38] to sample from the body's equilibrium distribution **B** and use these samples for Monte Carlo integration of Eq. 6. Importantly, the Metropolis-Hastings algorithm is able to sample from **B** using only the energy from Eq. 7, without having to compute the partition function of the Boltzmann distribution of Eq. 2.

There are computational advantages to modeling the distribution **B** at equilibrium. When the forces on the walker are conservative, **B** is translationally invariant, and depends only on the relative locations of the attached legs, and not on the whole system state $\omega = (P, A)$. When the walkers move over *regular* lattices, there are only a finite number of potential leg attachment gaits, and their corresponding attachment propensities can be precomputed, eliminating the need to run Metropolis-Hastings at every KMC iteration. This makes KMC simulation tractable for long times and large values of n. The details of the simulation of MVRWs on regular lattices can be found in previous work [35].

A. Random number generation

In all Monte Carlo methods the fundamental source of stochasticity derives from a deterministic pseudo-random number generator. The statistical properties of the pseudo-random number source are critically important to the correctness of model predictions [39]. To allow parallel computation and preserve mathematical guarantees of random number generator quality, we use the leapfrogging method to generate n parallel random number streams from a single master stream [40]. Hence, only a single random seed is needed to compute all n KMC traces for each set of model parameters studied.

B. Mean squared displacement and diffusion

In single-particle tracking, the stochastic motion of individual molecules is frequently analyzed in terms of the mean squared displacement (MSD) [41]. The MSD is the variance in the displacement, $\mathbf{Var}(\|\mathbf{p}(t)\|) = \langle \|\mathbf{p}(t)\|^2 \rangle$. For any diffusive process (i.e., an unbiased random walk) the MSD will scale linearly with time. Anomalous diffusion [42] is characterized by the MSD scaling as some non-linear power $0 \leq \alpha \leq 2$,

$$\langle \|\mathbf{p}(t)\|^2 \rangle \propto t^{\alpha}, \begin{cases} \alpha = 0 & \text{stationary} \\ 0 < \alpha < 1 & \text{subdiffusive} \\ \alpha = 1 & \text{diffusive} \\ 1 < \alpha < 2 & \text{superdiffusive} \\ \alpha = 2 & \text{ballistic or linear} \end{cases} . \quad (8)$$

MSD can either be computed as a temporal average (over different δt values for a single walker trajectory) or an ensemble average (over absolute t for an ensemble of trajectories from identical walker systems). Many biological systems are (or are at least assumed to be) *ergodic* in the sense that the motion of a walker is independent of its absolute position on the track and does not depend on its previous motion over a region of that track. Under the assumption of ergodicity the temporal and ensemble MSD are equivalent (assuming sufficient measurement resolution), but when a non-ergodic system is analyzed, only the ensemble average is meaningful for use in characterizing anomalous diffusion [43, 44]. MVRWs are a nonergodic system because they irreversibly modify the

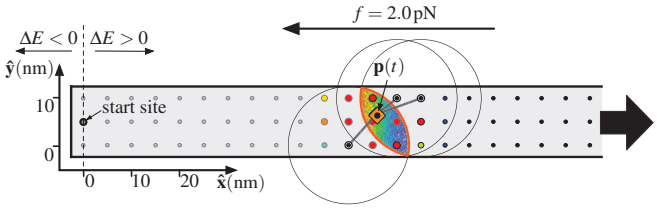

FIG. 4: (color online) A snapshot several hundred steps into a MVRW simulation. The surface track for walkers in this set of simulations consists of a semi-infinite strip of substrate sites 3-wide. Shown are the circular constraints imposed by the attached legs, and the probability density $p_{\mathbf{B}}$ for the body's equilibrium position (as a heat map). The walker has one unattached leg, and the relative rate at which it would attach to each site is shown by the size and color of the site. The boundary of the surface doesn't present any effective constraint on the walker's motion, other than the fact that the lack of sites outside the track prevents the walker body from moving more than a leg length, ℓ, into those empty regions.

track as they move over it. Thus, the motion of the walker depends on its absolute position on the track and specifically on whether the local sites are products or substrates. Hence, only the ensemble MSD can be used to study MVRWs.

IV. RESULTS

By itself a multivalent random walker is just a rather unsophisticated multivalent enzyme, but when paired with an appropriately designed nanoscale track of substrates it becomes a molecular transport device, able to move superdiffusively even under the influence of an external load force. Using KMC simulations we studied the motion of MVRWs moving over a 3-wide semi-infinite track of substrates (Fig. 4). The track spacing and other relevant parameters are summarized in Table I. As shown in Fig. 4, the walker starts with a single leg attached to the middle leftmost site at x-position 0. The remaining legs quickly attach, and the walker begins to move over the surface. From this initial position, the lack of substrates to the left breaks the symmetry of the walker's environment, and means the walker can only move in the $+\hat{\mathbf{x}}$ direction. The broken symmetry allows us to apply a load force to the walker's body in the $-\hat{\mathbf{x}}$ direction to oppose the walker's motion, and Eq. 7 describes the effect of that force on the walker body's energy function $U_{\mathbf{f}}$. If the force applied to the walker is $\mathbf{f} = (f_x, f_y)$, we let $f_y = 0$, and write $f = -f_x$ as a scalar for the magnitude of the force in the $-\hat{\mathbf{x}}$ direction. We limit $f \leq 4.0\,\mathrm{pN}$ as larger forces result in insignificant motion under the parameters of Table I. The upper bound of $f = 4.0\,\mathrm{pN}$ is near the maximum force a DNA-based realization of a MVRW could *a priori* be expected to move against, as the stall force for kinesin is approximately $5-8\,\mathrm{pN}$ [45], and the dissociation force for double-stranded DNA is $< 12\,\mathrm{pN}$ [46].

TABLE I: Model parameters used for simulations.

Parameter Description	Symbol	Value
Number of legs	k	4
Leg length	ℓ	12.5 nm
Track width	–	3 sites
Track length	–	semi-infinite
Track site spacing	–	$5.0\,\mathrm{nm} \times 5.0\,\mathrm{nm}$
Initial set of product sites	P	$\emptyset$
Effective substrate binding rate	k_{S}^{+}	$1.0 \times 10^3\,\mathrm{s}^{-1}$
Effective product binding rate	k_{P}^{+}	$1.0 \times 10^3\,\mathrm{s}^{-1}$
Substrate dissociation rate	k_{S}^{-}	$0.0\,\mathrm{s}^{-1}$
Product dissociation rate	k_{P}^{-}	$1.0\,\mathrm{s}^{-1}$
Catalysis rate	k_{cat}	$\leq 1.0\,\mathrm{s}^{-1}$
Temperature	T	300 K
Force in $-\hat{\mathbf{x}}$ direction	f	$\leq 4.0\,\mathrm{pN}$
Largest simulated time	$t_{\max}$	$\leq 1.0 \times 10^7\,\mathrm{s}$

A. The role of k_{cat} in walker kinetics

The chemical reactions from Eq. 1 describe the kinetics of a generic enzyme that can irreversibly transform substrates into products. From the modeling point of view all five reaction rates, k_{S}^{+}, k_{P}^{+}, k_{S}^{-}, k_{P}^{-}, and k_{cat} are free parameters that can each be varied to determine its effect on walker motion. In this work we focus on the special role that k_{cat} plays in controlling the walker's motion. Accordingly, we have fixed the values of the other four kinetic rates as shown in Table I, allowing us to study the effect of varying k_{cat}. We have fixed $k_{\mathrm{S}}^{+} = k_{\mathrm{P}}^{+}$ so that there is no attachment bias between substrates and products. This choice allows us to focus on the more subtle kinetic interplay of the remaining rates. Clearly a walker with $k_{\mathrm{S}}^{+} > k_{\mathrm{P}}^{+}$ will be more likely to attach to substrates than products as it is directly biased in attachment, and we investigate the effect of such kinetics in Sec. V E. However, we are primarily interested in investigating the minimal kinetic properties a MVRW must have in order to act as a molecular motor, and so we assume that $k_{\mathrm{S}}^{+} = k_{\mathrm{P}}^{+}$. With these rates equal, an unattached leg has no ability to differentiate between substrates and products and will just as rapidly bind to a feasible substrate as to a feasible product. Yet, even under these conditions a difference in the rates of k_{cat} and k_{P}^{-} can lead to a directional bias.

Consider that, once bound, a leg–product complex unbinds at rate k_{P}^{-}, and a leg–substrate complex unbinds at rate $k_{\mathrm{S}}^{-} + k_{\mathrm{cat}}$. We assume that substrate unbinding is much less probable than substrate catalysis so we let $k_{\mathrm{S}}^{-} = 0$ (the relaxation of this assumption is also considered in Sec. V E). Now, with $k_{\mathrm{cat}} = k_{\mathrm{P}}^{-}$, there is no residence time bias between substrates and products—the expected duration of a leg–product binding is the same as that for a leg–substrate binding. While substrates are still converted into products, the kinetics of the walker attachment and detachment are identical for both species. Hence, a walker with $k_{\mathrm{cat}} = k_{\mathrm{P}}^{-}$ is equivalent to a walker moving over an all-product surface. But an all-product surface provides no chemical free energy, and so an all-product walker system must move diffusively. Hence, a walker with $k_{\mathrm{cat}} = k_{\mathrm{P}}^{-}$ still releases chemical energy when

it catalyzes the conversion of a substrate, but the symmetrical kinetics prevent the walker from utilizing that energy. Thus in subsequent results we have fixed $k_{\mathrm{P}}^{-} = 1\,\mathrm{s}^{-1}$ while we vary k_{cat}, and the case where $k_{\mathrm{cat}} = 1\,\mathrm{s}^{-1} = k_{\mathrm{P}}^{-}$ represents the no-energy baseline motion of walkers. In contrast, when $k_{\mathrm{cat}} < 1\,\mathrm{s}^{-1} = k_{\mathrm{P}}^{-}$ there is a residence time bias, wherein leg–substrate bindings are longer in duration than leg–product bindings, as the leg must wait until the relatively slow catalysis step completes before it can unbind.

The only part of the walker kinetics that takes into account the chemical free energy released in substrate catalysis is the assumption of irreversibility in the enzymatic conversion from substrate to product. In enzyme kinetics there is some nonzero rate for the reverse of the catalytic process. However, if the Gibbs free energy (ΔG) drop from substrate to product is large enough, the reverse rate is so small it is for all practical purposes zero, and is omitted from the walker kinetics in our model (Sec. II A). Thus, we vary the k_{cat} parameter to control the residence time bias between visited and unvisited sites, and at $k_{\mathrm{cat}} = 1\,\mathrm{s}^{-1}$ the motion of the walker is *equivalent* to the no-free-energy case. We do not directly incorporate ΔG into the model, as the kinetic values of k_{cat} and k_{P}^{-} are more important to walker motion than ΔG, and any free energy change large enough to make the substrate modification effectively irreversible is sufficient to satisfy the model assumptions.

B. Walkers move superdiffusively in the absence of force

Figure 5 shows the ensemble estimates ($n = 1000$) for MVRWs moving in the absence of a load force. Initially (below the characteristic timescale of $1/k_{\mathrm{cat}}$) the walkers move subdiffusively. As expected, the $k_{\mathrm{cat}} = 1\,\mathrm{s}^{-1}$ walkers never move faster than diffusion. However, as k_{cat} is decreased, walkers initially move more slowly due to the the slower catalysis kinetics, but once sufficient time has passed, they move superdiffusively with $\alpha > 1$. The smaller the value of k_{cat}, the more superdiffusively the walkers move, with α approaching 2 for the smallest k_{cat} values. This superdiffusive behavior persists over several decades in time, during which the walkers move processively away from the origin in the direction of unvisited sites. Because of this outward-directed bias, the walkers with $k_{\mathrm{cat}} < 1\,\mathrm{s}^{-1} = k_{\mathrm{P}}^{-}$ eventually overtake (in MSD) the $k_{\mathrm{cat}} = 1\,\mathrm{s}^{-1}$ walkers given sufficient time. However, the ability to move superdiffusively depends on the local availability of the immobile substrate fuel, which is consumed as the walker moves over the track. Hence, if a walker moves back over previously visited sites, it becomes starved for fuel. In these energy-devoid regions the walker can only move diffusively like the $k_{\mathrm{cat}} = 1\,\mathrm{s}^{-1}$ walkers, and so superdiffusion must eventually give way to regular diffusion, even for the smallest values of k_{cat}.

Figure 6 shows $\langle N(t)\rangle$, the mean number of sites catalyzed by time t; its rate of change represents the average availability of substrate fuel. As long as the number of sites cleaved grows linearly with time, the walkers are receiving fuel at a constant rate and their motion is biased in the direction of

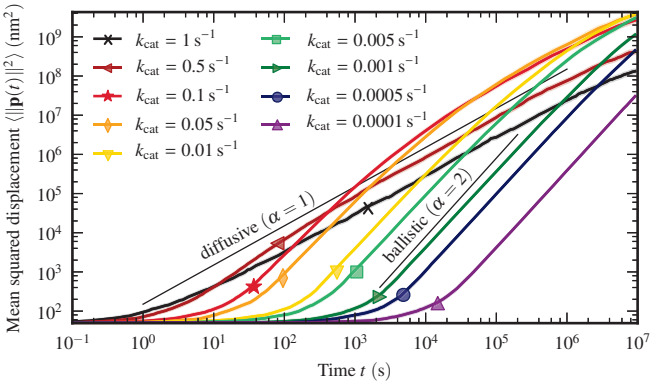

FIG. 5: (color online) Simulation estimate of $\langle\|\mathbf{p}(t)\|^2\rangle$ when $f = 0$. Walkers with $k_{\mathrm{cat}} = 1\,\mathrm{s}^{-1} = k_{\mathrm{P}}^{-}$ move diffusively. Those with $k_{\mathrm{cat}} < 1\,\mathrm{s}^{-1}$ move superdiffusively, but eventually use up their local supply of substrates and become ordinary diffusive. True transitions to diffusion will occur above simulated time $t_{\max} = 10^7$ s.

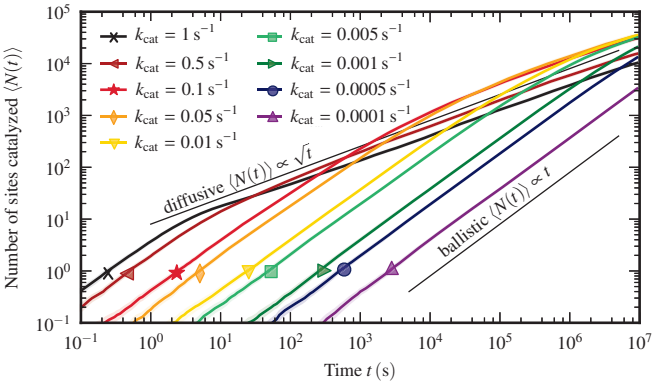

FIG. 6: (color online) Simulation estimate of $\langle N(t)\rangle$, the number of substrates catalyzed to products when $f = 0$. Since $k_{\mathrm{S}}^{-} = 0$, this is equivalent to the number of distinct sites visited at time t. Walkers with $k_{\mathrm{cat}} < 1\,\mathrm{s}^{-1}$ catalyze substrates at a nearly linear rate over many decades in time. This is necessary to maintain a constant supply of chemical energy to sustain superdiffusive motion.

new sites, which allows their constant fuel supply to be maintained. When $\langle N(t)\rangle$ becomes sub-linear the walkers begin to transition from superdiffusion to ordinary diffusion.

C. Walkers do work against a load

To quantify the sensitivity of the walker's superdiffusive motion, we impose a constant load force f on the walkers in the $-\hat{\mathbf{x}}$ direction (Fig. 4). Figure 7 shows ensemble ($n = 4000$) estimates of $\langle\|\mathbf{p}(t)\|^2\rangle$ under a range of forces for $k_{\mathrm{cat}} = 1\,\mathrm{s}^{-1}$ and $k_{\mathrm{cat}} = 0.01\,\mathrm{s}^{-1}$. Again, $k_{\mathrm{cat}} = 1\,\mathrm{s}^{-1} = k_{\mathrm{P}}^{-}$ (dashed lines) illustrates the no-energy case and, as shown previously (Fig. 5), walkers move diffusively without the influence of force.

When $f > 0$, the random walk over products is biased in the $-\hat{\mathbf{x}}$ direction. The lack of substrates to the left of the ori-

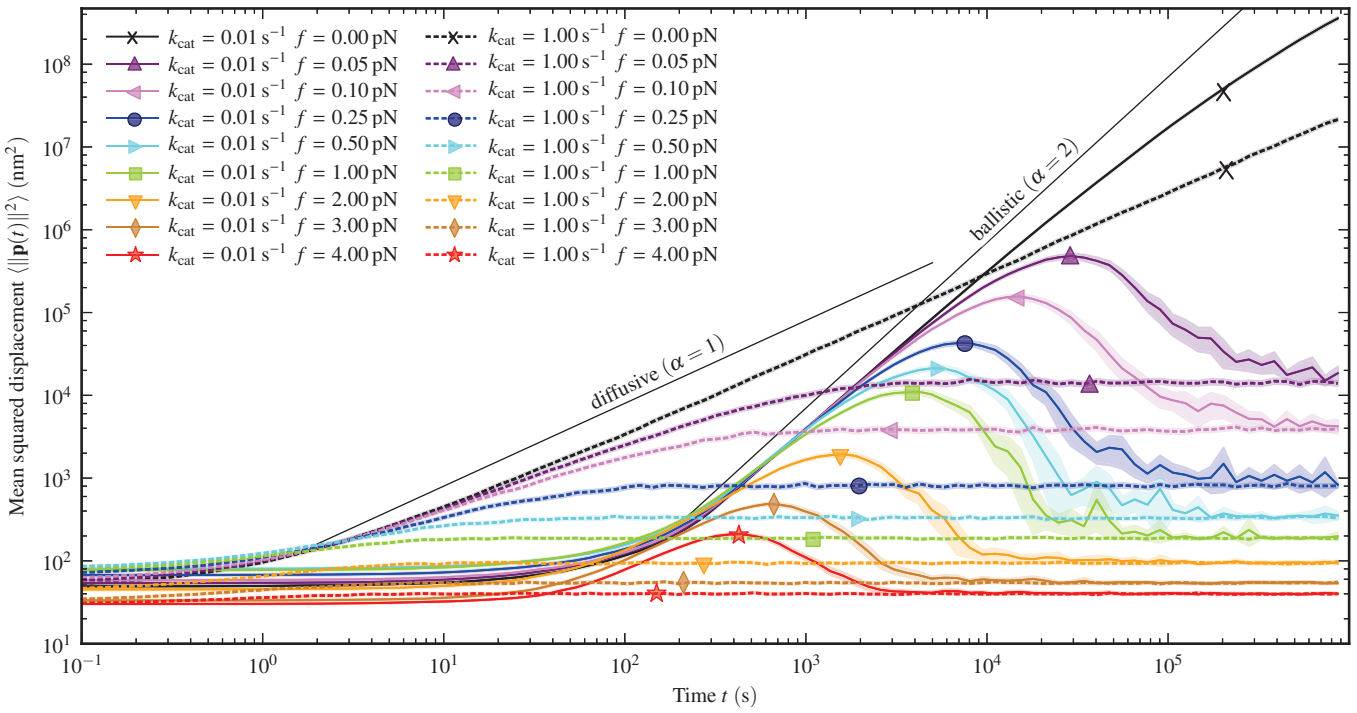

FIG. 7: (color online) Simulation estimate ($n = 4000$) of $\langle \|\mathbf{p}(t)\|^2 \rangle$ and 95% confidence bounds (shading) on a log-log scale. Reference lines are shown for ordinary diffusion ($\alpha = 1$) and ballistic motion ($\alpha = 2$). Walkers with $k_{cat} < 1\,s^{-1}$ move superdiffusively, but when $f > 0$, they eventually slow down and return to the same equilibrium position as the $k_{cat} = 1\,s^{-1}$ walkers.

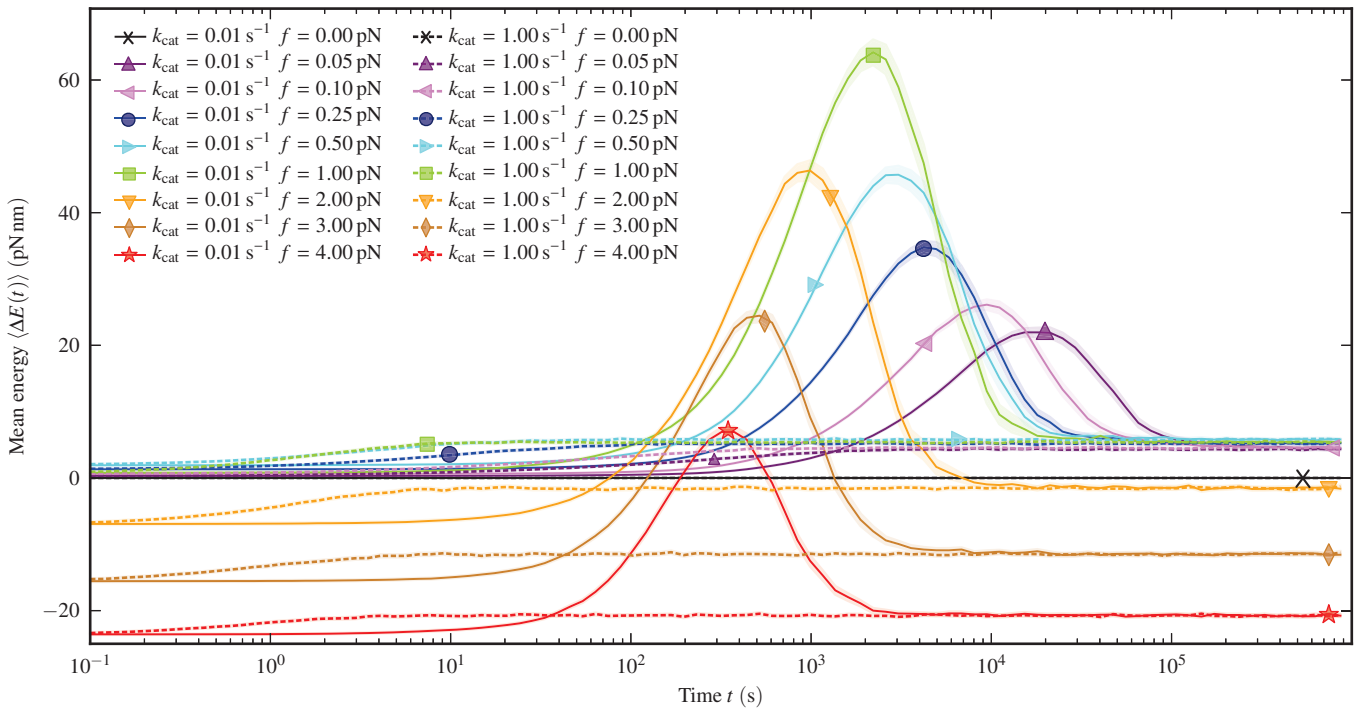

FIG. 8: (color online) Simulation estimate ($N = 4000$) of $\langle \Delta E(t) \rangle$ and 95% confidence bounds (shading) on a log-linear scale. Walkers with $f = 0$ always have $\Delta E = 0$. Those with $f > 0$ and $k_{cat} < 1\,s^{-1}$ do significant amounts of work, reaching a peak energy before eventually coming to an equilibrium. This equilibrium depends only on f and not on k_{cat}.

gin (Fig. 4) constrains the walker and the biased random walk will eventually reach an equilibrium position, after which the net motion is stationary ($\alpha = 0$). Indeed, this is seen for the $k_{\text{cat}} = 1\,\text{s}^{-1}$ walkers, which never move faster than diffusion, and their MSD increases monotonically to the equilibrium value exactly as if they were undergoing constrained diffusion in a box [47]. In contrast, when $k_{\text{cat}} < 1\,\text{s}^{-1}$ we again see nearly ballistic motion for all walkers except those under the highest load forces $f \geq 2.0\,\text{pN}$. Thus, even though the load force attempts to pull the walker body away from the substrate fuel, the long residence time for leg–substrate binding allows a few substrate-bound legs to resist the force and keep the walker in proximity to the substrate sites. Eventually, as in the $f = 0$ case, all walkers regardless of k_{cat} will exhaust their local supply of substrates and will find themselves moving over energy-devoid product sites, which ultimately brings them to the same equilibrium position as the $k_{\text{cat}} = 1\,\text{s}^{-1}$ walkers (for a given f).

The change in potential energy of the walkers (ΔE) as they move in opposition to the load force can be quantified by evaluating the ensemble estimate of the mean position of the walkers' bodies, $\langle \mathbf{p}(t) \rangle$. We chose to set $\Delta E = 0$ when $p_x = 0$, and then $\Delta E = f p_x > 0$ for walkers to the right of the origin (Fig. 4). Figure 8 shows the ensemble estimate of $\langle \Delta E(t) \rangle$. As the load force is increased above 0, the walkers attain progressively higher potential energies, and their peak energies come earlier, as they need to move less distance to do the same amount of work. However, as the forces are increased beyond $f = 2\,\text{pN}$, the walkers are not able to move very far without being pulled backwards, away from their substrate fuel, and they achieve only modest values of ΔE.

D. Walker velocity

Mean walker velocity is another useful measure of walker motility and is commonly used to characterize the motion of the processive cytoskelatal motors such as kinesin I and myosin V [48–50]. Estimation of mean velocity is difficult for multivalent random walkers because they do not operate in a steady state. Instead, like other measures of their motility, mean velocity is time dependent. Furthermore, the instantaneous velocity between steps has high variance.

In the experimental setup depicted in Fig. 4, we are interested in the mean velocity in the x direction, $\langle v_x(t) \rangle$, as this is the direction in which the force is applied. Velocity is not a directly observable quantity of the MVRW model, as walkers move in discrete steps over the state space. We can directly measure the mean position of the walker $\langle \mathbf{p}(t) \rangle = (\langle p_x(t) \rangle, \langle p_y(t) \rangle)$, which is defined as the mean location of the body position distribution $\langle \mathbf{B} \rangle$ (Eq. 2). Due to the variance of random variable $p_x(t)$, simple finite difference estimations of $\langle v_x(t_i) \rangle = (\langle p_x(t_{i+1}) \rangle - \langle p_x(t_i) \rangle)/(t_{i+1} - t_i)$ are too noisy with our sampled data.

In general, computing the derivative of a function known only with noisy measured data is an ill-posed problem and some sort of regularization procedure must be defined so that the solution can be uniquely determined [51]. The nature of the walker motion implies that the mean velocity should be a smooth function. Thus, we follow the methodology of Stickel [52] in which the problem is regularized by optimizing for a smooth interpolator $\hat{p}_x(t)$ that is both a good fit to the data and that has sufficiently small higher-order derivatives.

Stickel defines a functional Q that ranges over possible smooth interpolators φ on the interval $[t_0, t_{\max}]$,

$$Q(\varphi) = \int_{t_0}^{t_{\max}} |\varphi(t) - \langle p_x(t) \rangle|^2 \, \mathrm{d}t + \lambda \int_{t_0}^{t_{\max}} \left| \varphi^{(d)}(t) \right|^2 \mathrm{d}t. \quad (9)$$

In Eq. 9 the term $\int_{t_0}^{t_{\max}} |\varphi(t) - \langle p_x(t) \rangle|^2 \mathrm{d}t$ measures the $\mathcal{L}^2$-norm of the difference of the interpolator from the data, and the term $\int_{t_0}^{t_{\max}} |\varphi^{(d)}(t)|^2 \mathrm{d}t$ measures the $\mathcal{L}^2$-norm of the d-th derivative of φ. The smoothed position function, $\hat{p}_x(t)$, is the minimizer of the functional Q,

$$\hat{p}_x = \underset{\varphi}{\operatorname{argmin}} \, Q(\varphi), \quad (10)$$

and we can define the smoothed velocity as

$$\bar{v}_x(t) = \frac{\mathrm{d}}{\mathrm{d}t} \hat{p}_x(t). \quad (11)$$

The weighting parameter λ in Eq. 9 determines the relative importance we put on selecting a $\hat{p}_x(t)$ that minimizes the distance from the data $\langle p_x(t) \rangle$, versus a $\hat{p}_x(t)$ that has small d-th order derivative. As we are looking for the first derivative of $\hat{p}_x(t)$, we follow the advice of Stickel and optimize for $d = 3$, which is two more than the derivative we require an estimate for. We found that setting $\lambda = 100$ gave an optimal trade-off between accuracy and smoothness of the resulting derivative, and these results are shown in Fig. 9.

E. Peak work

When $f > 0$ all walkers eventually move to an equilibrium position with energy $\Delta E_\infty(f)$. This value is greater than the initial energy, because the walkers begin out of equilibrium with only a single leg attached (Fig. 4). The initial energy of the walker $\Delta E_0(f) < 0$, because we measure $\mathbf{p}$ as the body's equilibrium position $\langle \mathbf{B} \rangle$, which under any non-zero force will have $p_x < 0$ at the initial walker attachment location. However, the kinetics of $k_{\text{P}}^+ \gg k_{\text{P}}^-$ lead to an equilibrium where legs are almost always attached to a site, and because all sites are to the right of the origin, the equilibrium position $\Delta E_\infty(f)$ will also necessarily be greater than $\Delta E_0(f)$. Thus, to characterize the amount of useful work that a walker can do we take into account the equilibrium energy specific to each force. We define the peak work for force f as

$$w^\star(f) = \max_{t \in [0, t_{\max}]} \langle \Delta E(t; f) \rangle - \Delta E_\infty(f). \quad (12)$$

We estimate $\Delta E_\infty(f)$ as $\langle \Delta E(t_{\max}; f) \rangle$ for the $k_{\text{cat}} = 1$ walker. Figure 10a shows $w^\star$ as force and k_{cat} are varied. The $k_{\text{cat}} = 1\,\text{s}^{-1}$ walkers never have $w^\star > 0$, but the walkers with $k_{\text{cat}} < 1\,\text{s}^{-1}$ can do significant work under moderate forces.

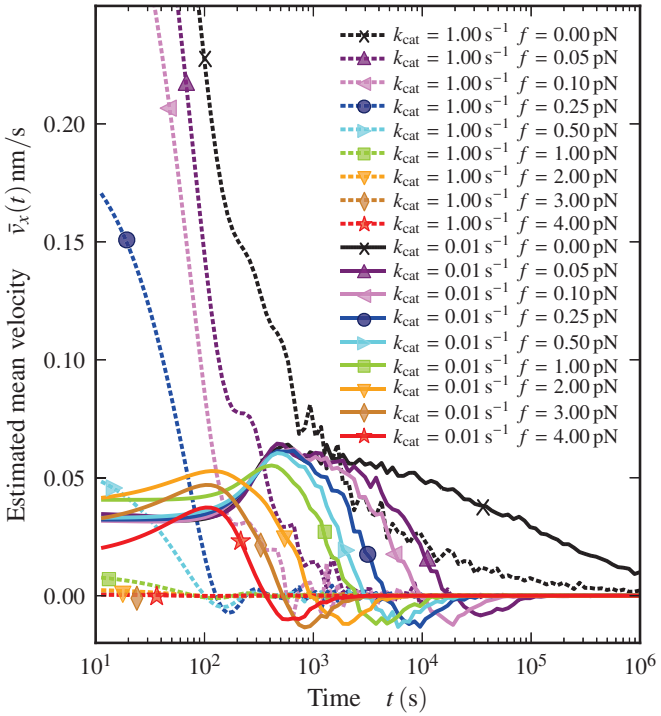

FIG. 9: (color online) The regularized finite difference estimate of the mean x-velocity, $\bar{v}_x(t)$, for walkers moving under load force f is based on smoothing of the ensemble estimate of $\langle p_x(t)\rangle$ ($n = 4000$). Results are shown for times $t \geq t_0 = 10\,\mathrm{s}$, as below this time the velocity mainly captures the effect of the high-frequency stepping of the walker between adjacent states in the state space. At longer times, we can clearly see the net positive velocity away from the origin experienced by the $k_{cat} < 1\,\mathrm{s}^{-1}$ walkers even under force. This net positive motion corresponds to the increase in walker energy $\Delta E(t)$ as shown in Fig. 8. The mean velocity approaches 0 as the walkers approach the constrained equilibrium imposed by the force.

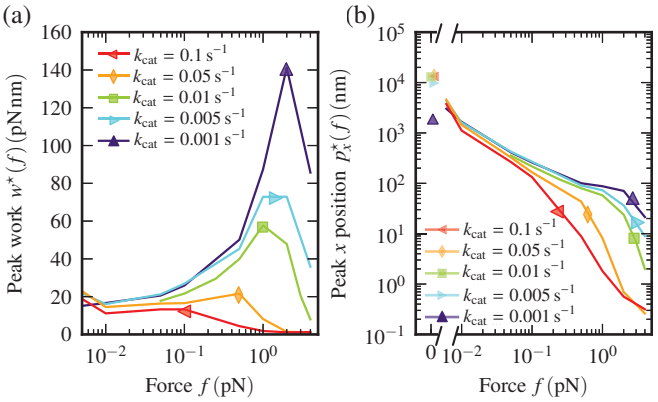

FIG. 10: (color online) Simulation estimate of (a) peak work $w^\star(f)$ and (b) peak x position $p_x^\star(f)$. Walkers with $k_{cat} \in \{1\,\mathrm{s}^{-1}, 0.01\,\mathrm{s}^{-1}\}$ are shown with an ensemble estimate of the mean using $n = 4000$ samples; other k_{cat} are shown using $n = 250$ samples. The peak position for $f = 0$ is shown as well, which is limited by the simulated time $t_{max} = 1.0 \times 10^6\,\mathrm{s}$. In particular when $f = 0$, the $k_{cat} = 0.001\,\mathrm{s}^{-1}$ walkers are still moving superdiffusively at $t = 1.0 \times 10^6\,\mathrm{s}$, but are limited by their slower stepping kinetics. At longer times the $k_{cat} = 0.001\,\mathrm{s}^{-1}$ walkers will achieve a peak position greater than those achieved by the larger k_{cat} walkers.

Figure 10b shows the values for the peak x-position,

$$p_x^\star(f) = \max_{t\in[0,t_{max}]} \langle p_x(t;f)\rangle - p_x^\infty(f). \tag{13}$$

Again we estimate the equilibrium x-position, $p_x^\infty(f)$ using $p_x(t_{max};f)$ as measured for the $k_{cat} = 1\,\mathrm{s}^{-1}$ walkers. These measurements show that the walkers move significantly farther under small loads, although they do nearly the same work.

V. DISCUSSION

Multivalent random walkers are able to do work because they act as Brownian ratchets. The physical motion of the walker is the result of random thermally driven molecular motions that are rectified by the constraints imposed by attached legs. Without any structural or conformational coupling, the independently operating legs are constrained only by their passive connection to a common body. The gaits with which MVRWs move are uncoordinated, unoriented, and acyclic, yet they can be designed to move nearly ballistically along tracks laid out in 2D.

From a thermodynamical perspective, the walkers are modeled as a closed system, where the only energy available to the walker is present in the uncleaved substrate sites. Any closed system will eventually approach a thermodynamic equilibrium after which no useful work can be accomplished. Indeed, we see this effect for the walkers under load force f shown in Figs. 7 and 8, where the walkers with $k_{cat} < k_P^-$ are able to move superdiffusively over significant distances and hence do work as they move in opposition to the load force, but they do so only while they still have energy available to bias their motion. Eventually, these walkers move to the same equilibrium distribution as the $k_{cat} = k_P^-$ walkers, which correspond to the no-energy case.

The key concept in the MVRW model of molecular walker motion is that energy is a local resource, and the walker depletes the local energy supply as it moves over a region and catalyzes the conversion of the substrate sites to products. This makes the MVRW system *non-ergodic* in the sense that the behavior of the walker depends on the local distribution of substrates and products, and this distribution in turn depends on the past motion of the walker over that region of the track. Most natural motors can be described as ergodic, as their fuel source (normally ATP) is present in solution and the track they move over is unmodified by their previous actions. Because MVRWs are non-ergodic they do not operate in a steady state, and unlike models of natural motors [29, 30] there is no way to quantify the motion of MVRWs by studying a particular set of cycles of states in their state space. As mentioned in Sec. III B, the non-ergodicity requires us to use the ensemble formulation of MSD. Additionally, most other random variables that describe MVRW motion ($\langle N(t)\rangle$, $\bar{v}_x(t)$, $\langle \Delta E(t)\rangle$, etc.) are time-dependent. Hence, there is no single value of velocity, or single stall force that can be calculated

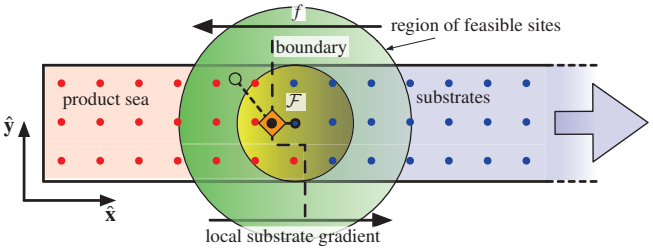

FIG. 11: (color online) The irreversible catalysis of substrates to products leads to the emergence of a spatial asymmetry in substrate concentration at the *boundary* between the contiguous *product sea* and the contiguous region of unvisited substrates. A walker with $k_{\text{cat}} < 1\,\text{s}^{-1}$ has a residence time bias where leg–substrate binding durations are much longer than for leg–product bindings. Thus, over time, legs are more likely to be attached to local substrates than local products, not because they seek out substrates, but because legs attached to products quickly detach. Hence, walkers are effectively driven in the direction of greatest local substrate density, and near the boundary this is always in the $+\hat{\mathbf{x}}$ direction. The irreversibility of substrate catalysis means the boundary itself also moves in the $+\hat{\mathbf{x}}$ direction, causing walkers near the boundary to move ballistically away from the origin.

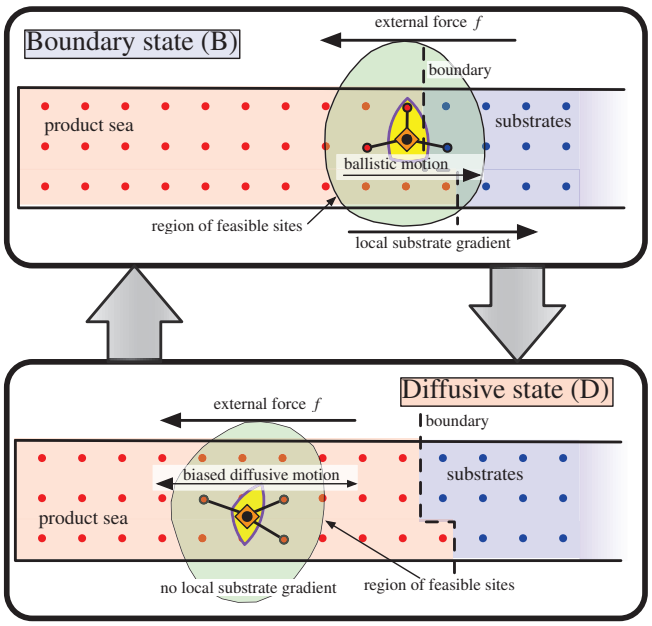

FIG. 12: (color online) The walker moves between boundary (*B*) and diffusive (*D*) metastates. The walker moves ballistically in the direction of local substrate gradient when in the *B* state, but moves diffusively over previously visited sites in the *D* state. The walker initially spends most of its time in the *B* state, consuming substrate fuel, however as the product sea grows, the time to exit the *D* state increases, leading to asymptotically diffusive motion in the absence of force and equilibrium stationary motion in the presence of force.

for MVRW-like systems, as is normally done for the ergodic motion of natural molecular motors [48].

A. Mechanism of superdiffusive motion

The superdiffusive motion of walkers and its eventual decay to diffusion ($f = 0$) or stationary equilibrium ($f > 0$) can be understood by noting that the only source of energy available to the walkers is present in the substrate molecules, which are a locally-limited, immobile resource.

After the walker starts moving and catalyzing sites, a contiguous region of product sites we call the *product sea* begins to form (Fig. 11). At the *boundary* between the product sea and unvisited substrates, the local substrate concentration gradient is in the $+\hat{\mathbf{x}}$ direction, due to the broken symmetry introduced by the semi-infinite surface configuration studied (Fig. 4). The emergence of spatial asymmetry in concentration makes it possible for an unoriented, symmetric walker to develop a directional bias. At the boundary, a MVRW with $k_{\text{cat}} < 1\,\text{s}^{-1}$ is biased in the $+\hat{\mathbf{x}}$ direction not because the legs are more likely to attach to substrates ($k_{\text{S}}^{+} = k_{\text{P}}^{+}$), but because when they do attach to a substrate, they stay bound longer—there is an effective *residence time bias.*

A walker with $k_{\text{cat}} < 1\,\text{s}^{-1}$ is only directionally biased when near the boundary, in which case its legs irreversibly catalyze attached substrates to products, moving the boundary in the $+\hat{\mathbf{x}}$ direction as well. Thus, as long as a walker remains near the boundary, it is biased in the $+\hat{\mathbf{x}}$ direction, and it moves the bias-inducing substrate concentration asymmetry along with it, which leads to persistent motion directed away from the origin.

This mechanism of residence time bias leading to a directional bias was identified by Antal and Krapivsky in their abstract 1D molecular spider model [13]. Later it was shown to lead to significant superdiffusive behavior of the Antal-Krapivsky (AK) walkers in 1D without force [14]. The simple state space of the AK walker models allows it to be shown analytically that the motion of AK walkers is ballistic in the direction of substrates while they remain proximate to the boundary [14]. The 2D geometry of the MVRW model makes the mathematical description of the boundary between substrates and products more complex, but with the simulation results in Figs. 5 and 7, we find the motion in 2D (at the ensemble level) is nearly ballistic even in opposition to small forces. This implies that individual walkers near the boundary must on average also be moving nearly ballistically, even under the effect of a constant load force.

B. The boundary and diffusive metastates

The emergence of the boundary between the product sea and the unvisited substrates causes the walker to move superdiffusively, but eventually all walkers either move diffusively ($f = 0$) or move to a stationary equilibrium distribution ($f > 0$). In analogy to our analysis of the AK spider model [14], this behavior can be understood by decomposing the Markov process into two metastates: a boundary state (*B*) wherein the walker is attached to substrates near the boundary, and a diffusive state (*D*) wherein the walker moves over

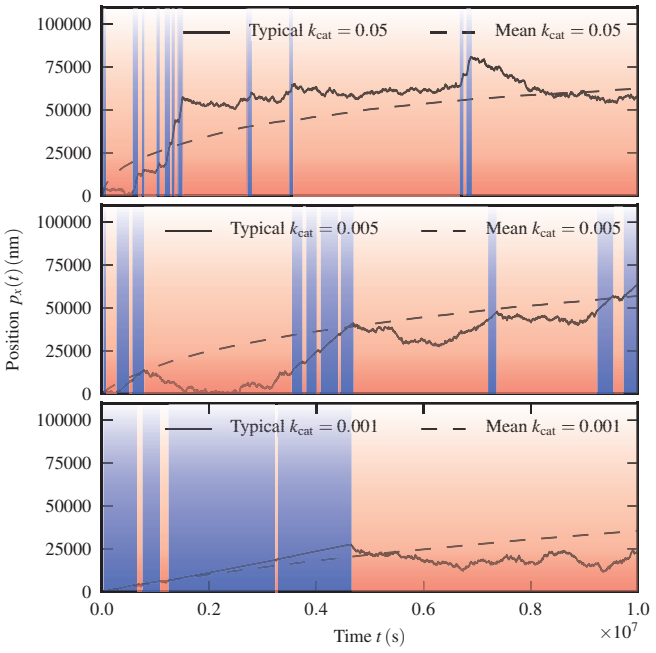

FIG. 13: (color online) Typical traces of $p_x(t)$ for a MVRW with $f = 0$ for three k_{cat} values. The traces are shaded darker (blue) when the walker is in the B metastate, and lighter (red) when it is in the D metastate. Walkers with smaller k_{cat} have longer B periods, but smaller velocity. The duration of B-periods is independent of time, but the duration of D-periods grows with the size of the product sea, and consequently increases over time. Thus, at short times the walker is more likely to be in the B state, but at longer times is more likely to be in the D state.

the energy-devoid product sea (Fig. 12).

When the walker is in the B state it moves ballistically in the $+\hat{\mathbf{x}}$ direction, but when it is in the D state it has no directional orientation, and it moves by ordinary unbiased diffusion for $f = 0$, or by $-\hat{\mathbf{x}}$-biased diffusion when $f > 0$. Figure 13 shows three typical traces of the position of individual walkers under no force, where B and D periods have been shaded to show the alternation between states and the distinction between the ballistic and diffusive motion.

The probability of a walker leaving the B state by moving sufficiently far in the $-\hat{\mathbf{x}}$ direction is independent of the absolute position of the boundary. Thus, the B metastate is Markovian since the transition rate to the D metastate is independent of how long the walker has been moving or the size of the product sea. As k_{cat} is decreased, the duration of leg–substrate bindings relative to leg–product bindings increases and the walker is less likely to simultaneously detach from all boundary substrates and leave the B state. Thus, lower k_{cat} values result in more persistent ballistic motion over longer durations, but at smaller velocities (Fig. 13).

In contrast the D metastate is non-Markovian. The duration of a D period depends on the size of the product sea, and hence this duration grows as the walker catalyzes sites. In the case where $f = 0$, the time is quadratically dependent on the size of the product sea, but when $f > 0$ this dependence becomes exponential, and for sufficient forces and sufficiently sized product seas, the probability of returning to the boundary once departed a significant distance becomes effectively nil. Hence, the duration of B-periods is constant in time, but the duration of D-periods grows. Eventually walkers spend nearly all their time moving over products in the D state, and so approach the same equilibrium distribution as the $k_{cat} = 1\,\mathrm{s}^{-1}$ walkers which represent the case where no energy is available to the walker. This eventual drift toward equilibrium can be seen in Figs. 7 and 8.

C. Dissociation

There is a non-zero probability for a walker to detach from the track if $k-1$ legs are simultaneously in the detached state, and the next action chosen is for the remaining leg to detach. A walker with k detached legs is free to diffuse in solution, and cannot be ascribed a well-defined position with a discrete state Markov process. Hence, dissociation poses mathematical difficulties for analyzing a non-ergodic motive process and comparing it with other mathematical models of anomalous diffusion. Ergodic models of natural motors like kinesin I can simultaneously analyze motion and dissociation, because the transport characteristics and dissociation probabilities can be understood independently by studying a single motor cycle [30, 53]. MVRWs, being non-ergodic, have transport and dissociation probabilities that depend on the current state of the local chemical sites, and cannot be analyzed with similar techniques.

One approach to dealing with dissociation in non-ergodic walker models is to have a single absorbing dissociated state to which all walkers will eventually go and never return. This state is then the single equilibrium state of the system, and analysis is done on the remaining walkers. However, analyzing MSD becomes challenging because at any $t > 0$ there is necessarily some non-zero proportion of walkers in the dissociated state. Ensemble MSD is no longer well-defined, as we cannot ascribe a position to dissociated walkers. Instead of this approach, we implement a *hopping rule*, whereby a walker with $k-1$ legs whose next KMC chosen transition is to detach its one remaining leg is prevented from diffusing away from its dissociation location. It is temporarily held in place until a leg attaches to a local feasible site. The net effect is a hop from one site to another, and it is implemented as a single KMC step, so that the position of the walker is always well defined.

For any finite k_S^+ and k_P^+ rates, it is possible for walkers to temporarily dissociate via a hopping event. In practice, however, when the walker has sufficiently many legs, the on-rates are sufficiently fast, the legs are long, and the substrates are densely spaced, the probability of dissociation is low. Over the course of the simulations shown in Figs. 7 and 8, only four out of 56000 walkers with $f < 3.0\,\mathrm{pN}$ and 100 out of 16000 walkers with $f \geq 3.0\,\mathrm{pN}$ experienced any hopping event.

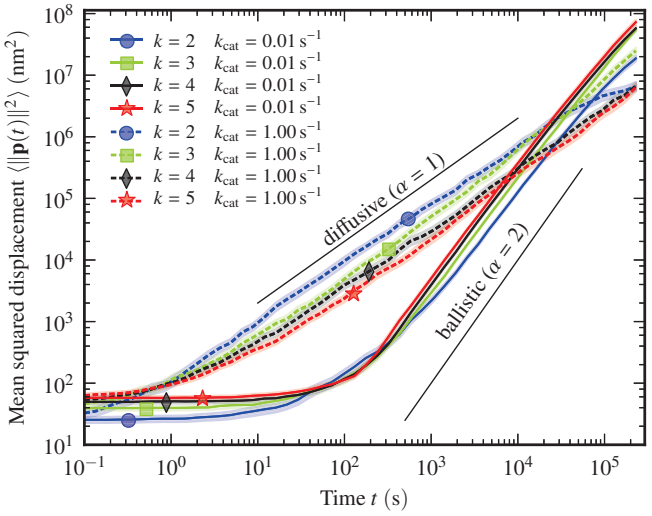

FIG. 14: (color online) Simulation estimates ($n = 400$) showing the effect of the number of walker legs (k) on walker motion when $f = 0$. The MSD is shown with 95% confidence intervals in shading. Walkers with more legs move with smaller diffusion constant when $k_{cat} = 1\,s^{-1} = k_p^-$ and there is no residence time bias. However, when $k_{cat} = 0.01\,s^{-1}$, the walkers with more legs experience a stronger directional bias towards the local substrate concentration gradient and hence move superdiffusively over longer times and distances. Of the configurations studied, walkers with $k = 5$ legs and $k_{cat} = 0.01\,s^{-1}$ eventually achieve the greatest mean squared displacement. The black lines show the case $k = 4$, corresponding to walkers in Fig. 5.

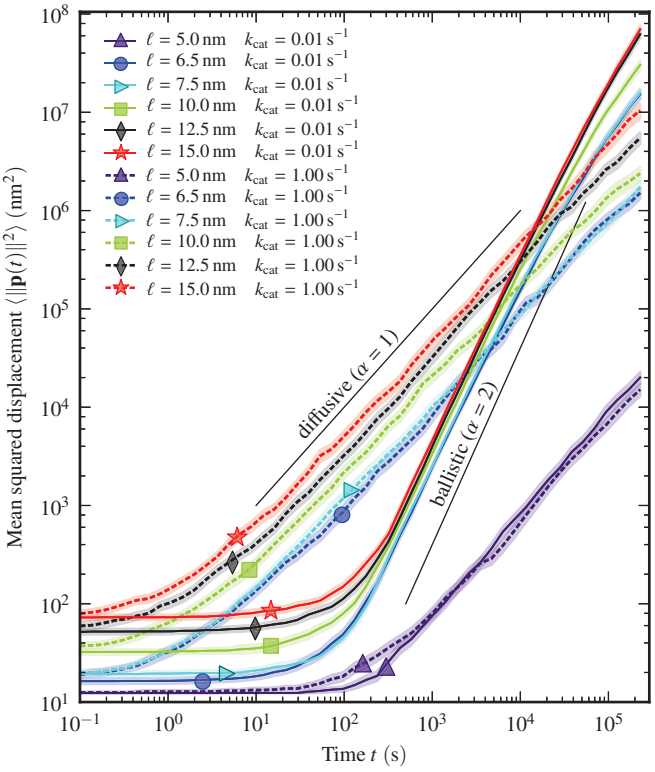

FIG. 15: (color online) Simulation results ($n = 400$) showing the effect (at $f = 0$) of varying the leg length 5.0 nm $\leq \ell \leq$ 15.0 nm, while the number of legs is fixed at $k = 4$ and the substrate spacing is fixed at 5.0 nm $\times$ 5.0 nm. The effect of ℓ on MSD is shown with shading indicating the 95% confidence interval for the mean. The effect of changing the leg length is essentially manifested as a change in the diffusion constant, but not in the qualitative characteristics of the superdiffusive motion for the $k_{cat} = 0.01\,s^{-1}$ walkers. The exception is for the very short leg length $\ell = 5.0$ nm, where the average number of feasible sites becomes so small that walkers lose their superdiffusive transport behavior

D. Effect of variation of number of legs and leg length

As summarized in Table I, our results focus on four-legged walkers with leg length $\ell = 12.5$ nm, which is 2.5 times the 5.0 nm substrate spacing distance. Both the leg length and the number of legs can be freely varied. However, there are sensible ranges for these parameters, outside of which the motion of the walkers is not as processive, or is exceedingly slow. To be efficient molecular transport devices, walkers must simultaneously avoid dissociation, resist the effect of forces, and remain attached to substrates near the boundary.

First, consider the number of legs, which is varied in the range $2 \leq k \leq 5$ in Fig. 14. For the residence time bias to lead to a directional bias, we require $k \geq 2$ [14]. With few legs ($k = 2$), walkers are more likely to have all of their legs detached simultaneously and undergo a hopping step. As the number of legs is increased this probability drops exponentially, as each leg's probability of detachment is approximately independent. Walkers with more legs also tend to move more superdiffusively and processively when in the B state, as they have a higher probability that at least one leg remains attached to a substrate at the boundary. However, we find walkers with many legs have a significantly smaller diffusion constant. This observation agrees with the calculations of Antal and Krapivsky regarding the relationship of the number of legs and the effective diffusion constant of walkers in the AK spider model [12, 13]. Due to these considerations, $k = 4$ was chosen as a reasonable compromise value that prevents dissociation, maintains a strong tendency to remain on the boundary, and moves with an appreciably fast diffusion constant.

The leg length, ℓ, can also be freely varied, but it must be considered in relation to the substrate spacing. Together these parameters determine the average number of feasible sites available for attachment. Ideally, the substrate spacing would be made as small as possible, but it is constrained by limits on the sizes of molecules and how closely substrates can be arrayed on a surface. We chose 5.0 nm as a reasonable lower limit on this spacing, as it approximates the density of DNA substrates arrayed on a DNA origami [54] surface, as employed in molecular spider experiments [11].

Figure 15 shows the effect of varying the leg length for 4-legged walkers while keeping the substrate spacing constant at 5.0 nm. We find that if legs are too short ($\ell \leq 5.0$ nm), the number of feasible sites is too small to maintain a superdiffusive effect. For leg lengths $\ell \geq 7.5$ nm, which is 1.5 times the substrate spacing, there is little qualitative difference in the

walker motion, although longer legs do lead to a faster diffusion constant in the absence of force.[2] Under load, however, leg length and substrate spacing should both be minimized to maximize the peak work and displacement of walkers. Longer legs allow a larger feasible region $\mathcal{F}$, leading to a larger bias in **B** under any non-zero load. This in turn makes it more likely for long-legged walkers to move backwards. We found that a leg length of approximately 2.5 times the substrate spacing provides a good balance between dissociation and processivity; a full analysis of this relationship is reserved for future study.

E. Sensitivity to kinetic parameters

We initially arrived at the MVRW model through our efforts to predict the characteristics of molecular spider motion in laboratory experiments (e.g., experiments like those of Lund et al. [11] in which spiders moved over nano-fabricated tracks of substrates). Hence, the MVRW model is built around the chemically realistic kinetics given in Eq. 1 which model the dexyribozyme-based molecular spiders' legs [9]. Until now we have assumed that most of these rates are fixed, and have shown that varying just the $k_{\text{cat}}/k_{\text{P}}^{-}$ ratio suffices to create a residence time bias that leads to superdiffusive motion. While a truly minimalist model of uncoordinated enzymatic walkers could be distilled from the MVRW model by assuming that attachment rates are infinite (thus eliminating the parameters k_{S}^{+} and k_{P}^{+}), and the conclusions of Sec. IV and the analysis of the mechanism of superdiffusion in Sec. V A would still hold, we have maintained the model's foundation in finite rates and realistic enzyme kinetics. This decision to keep all rates finite does not make the model any more complicated to simulate, but it does make a full exploration of the parameter space a more challenging endeavor. For this reason, we have until now fixed the kinetic rates other than k_{cat}, as summarized in Table I.

Now, we consider the effect of the variation of these other kinetic parameters on the superdiffusive effect that has been demonstrated for our fixed rates. The sensitivity of walker motion to these kinetic rates is critical to our characterization of the MVRWs as molecular motors, because any chemical implementation of the multivalent random walker model (e.g., molecular spiders) will have finite rates, and they will potentially vary considerably from those in Table I. However, we show that the qualitative characteristics of superdiffusive walker motion persist over a wide range of kinetic values, as long as the fundamental kinetic feature of a residence time bias between visited and unvisited sites is present. This residence time bias is ultimately what leads to an effective motive bias in the direction of the local substrate concentration gradient, and allows the walker to function as a molecular motor.

[2] A similar relationship between effective leg length and diffusion constant was also calculated by Antal and Krapivsky for their AK-model walkers [12, 13].

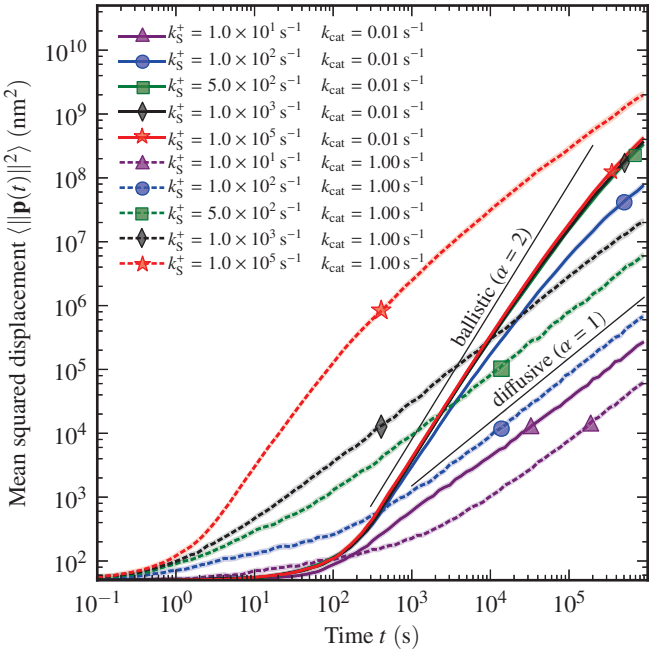

FIG. 16: (color online) Simulation results ($n = 1000$) showing the effect (at $f = 0$) of varying k_{S}^{+} on the MSD of walkers while k_{P}^{+} is fixed at $1.0\times10^3\,\text{s}^{-1}$. The black lines represent the case where $k_{\text{P}}^{+} = k_{\text{S}}^{+} = 1.0\times10^3\,\text{s}^{-1}$, which is used in all other simulations results. When $k_{\text{P}}^{+} = k_{\text{S}}^{+}$, there is no attachment preference for a substrate over a product. An unattached leg will just as rapidly bind to a feasible substrate as to a feasible product. However, as we take $k_{\text{S}}^{+} < k_{\text{P}}^{+}$, the walkers have an attachment bias to products, which should be expected to reduce the time spent in the boundary (B) metastate, and therefore lead to less pronounced superdiffusive behavior. These results show that the MSD is robust to moderate changes in the on-rates, and even for $k_{\text{S}}^{+} = k_{\text{P}}^{+}/10$, there is an appreciable superdiffusive effect when $k_{\text{cat}} = 0.01\,\text{s}^{-1}$. However taking $k_{\text{S}}^{+} = k_{\text{P}}^{+}/100$ overwhelms the residence time bias of the walkers in the B state and prevents any superdiffusive motion.

In Fig. 16 we show that the superdiffusive behavior as quantified by MSD persists over an order of magnitude in variation of the k_{S}^{+} rate. Indeed, even in the pessimistic case where the walker is biased 10:1 in attachment preference to products over substrates, the residence time bias of 100:1 of substrate to product binding duration is still sufficient to achieve a superdiffusive scaling of MSD over several decades in time. This robustness even to large changes in attachment rates allows us to be confident that superdiffusive behavior is a pervasive feature of multivalent random walker systems and is not critically dependent on our particular choice of attachment rates.

We show the results of varying k_{S}^{-} in Fig. 17. In other results we have assumed that $k_{\text{S}}^{-} = 0$, which is reasonable as this rate is likely to be much slower than k_{P}^{-} or k_{cat} for any practical enzymatic implementation of a multivalent random walker. Figure 17 shows that indeed the superdiffusive behavior is robust to changes in k_{S}^{-}, as long as it remains significantly slower than k_{P}^{-} and k_{cat}. However, setting $k_{\text{S}}^{-} = k_{\text{P}}^{-}$

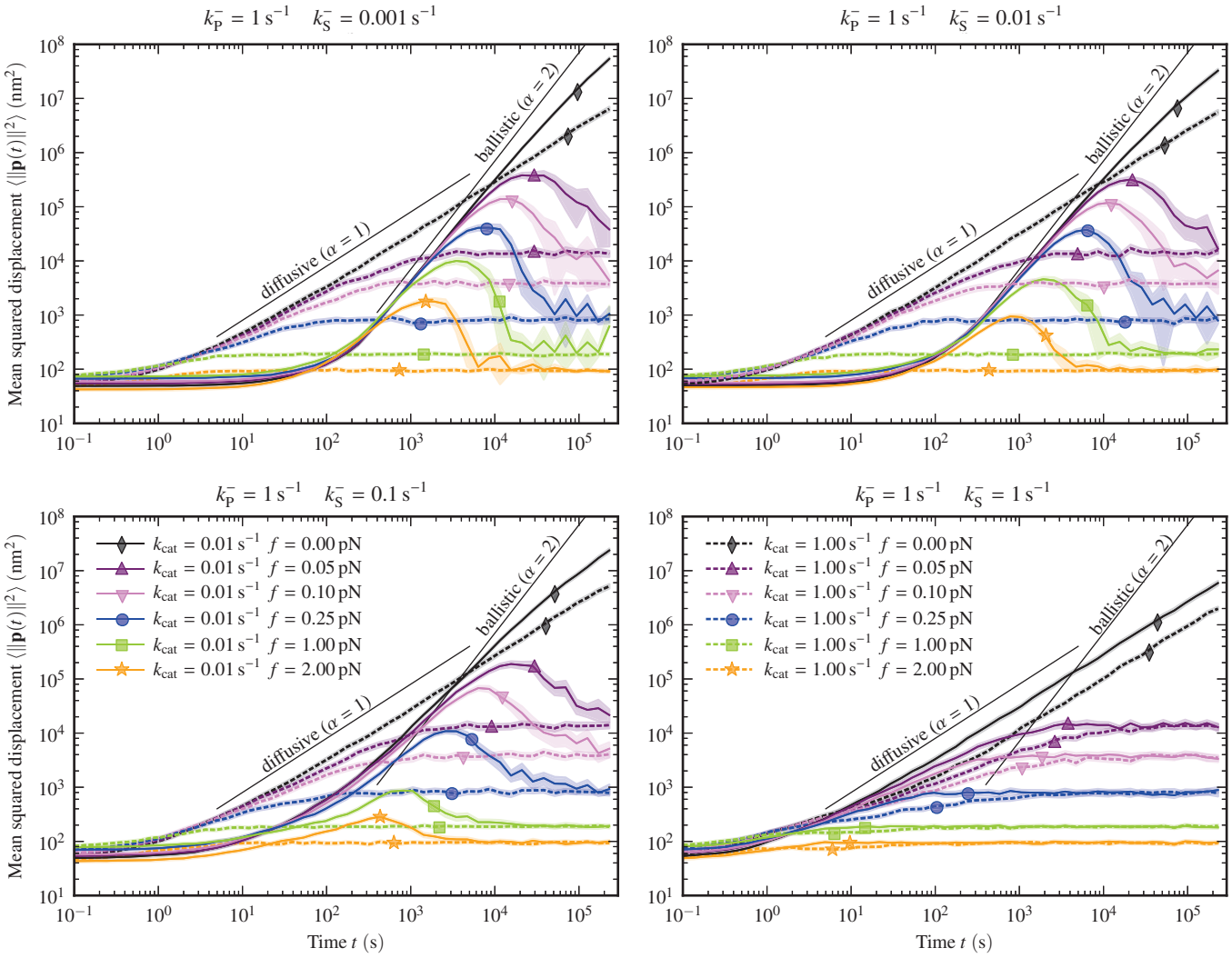

FIG. 17: (color online) Simulation estimates ($n = 1000$) of the mean squared displacement of the walkers as k_S^- is varied. Shading shows 95% confidence intervals for the mean. Each subplot shows the same 12 walker configurations, varying only the values of k_S^-. Fiducial lines for diffusion and ballistic motion are shown in the same position on each subplot for reference. These data can be compared with Figure 7 which shows the case $k_S^- = 0$. The value of k_S^- determines the rate of detachment without enzymatic conversion of the site to a product. As long as $k_S^- + k_{cat} < k_P^-$, there remains a residence time bias, and our results show that walkers with $k_{cat} = 0.01\,s^{-1}$ move superdiffusivly for $k_S^- < k_P^- = 1\,s^{-1}$. This shows that the qualitative behavior of the walkers is unchanged for small variations in k_S^-, and the choice of $k_S^- = 0$ in the model is appropriate because small values of k_S^- do not significantly affect the walker motion. However, when $k_P^- = k_S^- = 1\,s^{-1}$ the superdiffusive motion is eliminated, as there is no longer an effective residence time bias between visited and unvisited sites.

eliminates any superdiffusive effect, as there is no longer a residence time bias between substrates and products, and the motion of the walker near the boundary is no longer biased in the direction of the local substrate concentration gradient.

F. Effect of forces on dissociation reactions

In describing our model we show how forces affect the bimolecular association rates through Eq. 6. However, applying a load force to walkers should also affect the kinetics of the unimolecular dissociation events. From a high-level view, the kinetics of unimolecular reactions depend on a molecule having enough internal energy to surmount some reaction energy barrier U_0. Thus, rate laws follow the Arrhenius formula, $k(T) \propto \exp(-U_0/k_BT)$. The effect of a force f applied to the molecule is a mean change in energy of ΔU_f, and the rate is modified to

$$k(T) = \nu \exp\left((\Delta U_f - U_0)/k_BT\right). \tag{14}$$

The value of the constant ν and the relationship of ΔU_f with force f depend on the specific internal chemistry of the leg tethers, enzymes, and substrates [55–57], the details of which are beyond the scope of our coarse-grained walker model. We surmise that the effect of small forces is a slight increase in

k_S^- and k_P^-, although this change would not be uniform over all legs, as those attached to sites further in the $+\hat{\mathbf{x}}$ direction will oppose more of the load force on average than other sites. Based on Fig. 17, small increases in k_S^- do not qualitatively change the motive properties of the walker with regard to MSD, except when the forces are large enough that $k_S^- + k_{cat} \geq k_P^-$, which eliminates the residence time bias and all superdiffusive motion. Additionally, small increases in k_P^- actually lead to an increase in the MSD, as they increase the residence time bias. Quantitative analysis of variation in k_P^- is beyond the scope of this paper, but is available along with other supplementary results for the MVRW model [35]. Overall, these results show that even though the present formulation of the MVRW model does not describe the effect of force on dissociation rates, we expect an extension of the model including these rates to predict similar superdiffusive behaviors, as long as the forces and corresponding rate changes are small.

VI. CONCLUSION

The multivalent random walker model describes walker systems that can be designed to act as translational molecular motors, without the need for complex intra-molecular conformational switching or gaiting. Unlike models of natural molecular motors such as kinesin I and myosin V [25, 29, 30], we do not assume any coordination between the legs, chemical or mechanical. Instead, we assume that the legs act independently. The legs are passively constrained by their tethering to a common body, but the chemical state of one leg cannot be communicated to the other legs. We show that such a simple walker design is able to exploit a residence time bias in the enzymatic kinetics of the substrate and product sites it moves over to generate a directional bias. In addition, because the substrate sites take the dual role of the chemical fuel source and the track binding sites, there is no need to couple together in each foot a separate track binding and fuel binding site, as in kinesin I and other natural motors [1]. Hence, these difficult-to-engineer features that are found in natural molecular motors are not strictly necessary for MVRW-like walkers to transduce the chemical free energy of substrate catalysis into physical work, and many enzyme–substrate systems could provide the effective kinetics necessary for a multivalent random walker to act as a molecular motor. For this reason we avoid explicitly focusing on a particular enzyme–substrate system in the MVRW model and instead we explain how the interplay between the various kinetic rates controls the ability of a multivalent random walker to act as a molecular motor, transforming chemical free energy into directed motion and performing physical work as it moves in opposition to a load force.

Acknowledgments

The authors would like to thank Tibor Antal, Thomas P. Hayes, Paul L. Krapivsky, Cristopher Moore, Milan N. Stojanovic, and Lance R. Williams for helpful discussions and advice regarding the development of our model and simulation software, and the analysis and interpretation of results. This material is based upon work supported by the National Science Foundation under grants 0533065, 0829896, and 1028238.

[1] R. D. Vale and R. A. Milligan, Science **288**, 88 (2000).
[2] K. Svoboda, C. F. Schmidt, B. J. Schnapp, and S. M. Block, Nature **365**, 721 (1993).
[3] C. M. Coppin, J. T. Finer, J. A. Spudich, and R. D. Vale, Proc. Nat. Acad. Sci. USA **93**, 1913 (1996).
[4] E. R. Kay, D. A. Leigh, and F. Zerbetto, Angew. Chem. Int. Ed. **46**, 72 (2007).
[5] A. Agarwal and H. Hess, Prog. Polym. Sci. **35**, 252 (2010).
[6] K. S. Thorn, J. A. Ubersax, and R. D. Vale, J. Cell Bio. **151**, 1093 (2000).
[7] M. Tomishige, N. Stuurman, and R. D. Vale, Nat. Struct. Mol. Bio. **13**, 887 (2006).
[8] E. Toprak, A. Yildiz, M. T. Hoffman, S. S. Rosenfeld, and P. R. Selvin, Proc. Nat. Acad. Sci. USA **106**, 12717 (2009).
[9] R. Pei, S. K. Taylor, D. Stefanovic, S. Rudchenko, T. E. Mitchell, and M. N. Stojanovic, J. Am. Chem. Soc. **39**, 12693 (2006).
[10] M. Bonaccio, A. Credali, and A. Peracchi, Nucleic Acids Res. **32**, 916 (2004).
[11] K. Lund, A. J. Manzo, N. Dabby, N. Michelotti, A. Johnson-Buck, J. Nangreave, S. Taylor, R. Pei, M. N. Stojanovic, N. G. Walter, et al., Nature **465**, 206 (2010).
[12] T. Antal, P. L. Krapivsky, and K. Mallick, J. Stat. Mech. **2007**, P08027 (2007).
[13] T. Antal and P. L. Krapivsky, Phys. Rev. E **76**, 021121 (2007).
[14] O. Semenov, M. J. Olah, and D. Stefanovic, Phys. Rev. E **83**, 021117 (2011).
[15] C. Gallesco, S. Müller, and S. Popov, ESAIM: Probab. Stat. **15**, 390 (2011).
[16] C. Gallesco, S. Müller, S. Popov, and M. Vachkovskaia, ALEA: Lat. Am. J. Probab. Math. Stat. **8**, 129 (2011).
[17] I. Ben-Ari, K. Boushaba, A. Matzavinos, and A. Roitershtein, Bull. Math. Biol. **73**, 1932 (2011).
[18] T. Antal and P. L. Krapivsky, Phys. Rev. E **85**, 061927 (2012).
[19] O. Semenov, M. J. Olah, and D. Stefanovic, in *DNA Computing and Molecular Programming* (Springer Berlin / Heidelberg, 2011), vol. 6937 of *Lecture Notes in Computer Science*, pp. 204–216.
[20] O. Semenov, M. J. Olah, and D. Stefanovic, Nat. Comput. (2012).
[21] M. Rank, L. Reese, and E. Frey, Phys. Rev. E **87**, 032706 (2013).
[22] L. Samii, H. Linke, M. J. Zuckermann, and N. R. Forde, Phys. Rev. E **81**, 021106 (2010).
[23] L. Samii, G. A. Blab, E. H. C. Bromley, H. Linke, P. M. G. Curmi, M. J. Zuckermann, and N. R. Forde, Phys. Rev. E **84**, 031111 (2011).
[24] A. Yildiz, M. Tomishige, A. Gennerich, and R. D. Vale, Cell

134, 1030 (2008).
[25] E. M. Craig and H. Linke, Proc. Nat. Acad. Sci. USA **106**, 18261 (2009).
[26] C. S. Peskin, G. M. Odell, and G. F. Oster, Biophys. J. **65**, 316 (1993).
[27] D. T. Gillespie, J. Comput. Phys. **22**, 403 (1976).
[28] D. Keller and C. Bustamante, Biophys. J. **78**, 541 (2000).
[29] S. Liepelt and R. Lipowsky, Phys. Rev. Let. **98**, 258102 (2007).
[30] R. D. Astumian, Biophys. J. **98**, 2401 (2010).
[31] V. Bierbaum and R. Lipowsky, Biophys. J. **100**, 1747 (2011).
[32] A. B. Bortz, M. H. Kalos, and J. L. Lebowitz, J. Comput. Phys. **17**, 10 (1975).
[33] A. Voter, in *Radiation Effects in Solids*, edited by K. Sickafus, E. Kotomin, and B. Uberuaga (Springer, 2007).
[34] M. J. Olah and D. Stefanovic, in *DNA Computing and Molecular Programming* (Springer Berlin / Heidelberg, 2011), vol. 6937 of *Lecture Notes in Computer Science*, pp. 160–174.
[35] M. J. Olah, Ph.D. thesis, University of New Mexico (2012).
[36] N. Metropolis and S. Ulam, J. Am. Stat. Assoc. **44**, 335 (1949).
[37] N. Metropolis, A. W. Rosenbluth, M. N. Rosenbluth, A. H. Teller, and E. Teller, J. Chem. Phys. **21**, 1087 (1953).
[38] W. K. Hastings, Biometrika **57**, 97 (1970).
[39] A. M. Ferrenberg, D. P. Landau, and Y. J. Wong, Phys. Rev. Let. **69**, 3382 (1992).
[40] H. Bauke and S. Mertens, Phys. Rev. E **75**, 066701 (2007).
[41] W. Ying, G. Huerta, S. Steinberg, and M. Zúñiga, Bull. Math. Bio. **71**, 1967 (2009).
[42] S. Havlin and D. Ben-Avraham, Adv. Phys. **51**, 187 (1987).
[43] A. Lubelski, I. M. Sokolov, and J. Klafter, Phys. Rev. Let. **100**, 250602 (2008).
[44] J.-H. Jeon and R. Metzler, Phys. Rev. E **85**, 021147 (2012).
[45] K. Visscher, M. J. Schnitzer, and S. M. Block, Nature **400**, 184 (1999).
[46] B. Essevaz-Roulet, U. Bockelmann, and F. Heslot, Proc. Nat. Acad. Sci. USA **94**, 11935 (1997).
[47] K. Ritchie, X.-Y. Shan, J. Kondo, K. Iwasawa, T. Fujiwara, and A. Kusumi, Biophys. J. **88**, 2266 (2005).
[48] C. M. Coppin, D. W. Pierce, L. Hsu, and R. D. Vale, Proc. Nat. Acad. Sci. USA **94**, 8539 (1997).
[49] J. Howard, Nature **389**, 561 (1997).
[50] M. Nishiyama, H. Higuchi, and T. Yanagida, Nat. Cell Bio. **4**, 790 (2002).
[51] C. R. Vogel, *Computational methods for inverse problems* (Siam, Philadelphia, Pa, 2002).
[52] J. J. Stickel, Comput. Chem. Eng. **34**, 467 (2010).
[53] R. Lipowsky and S. Liepelt, J. Stat. Phys. **130**, 39 (2008).
[54] P. W. K. Rothemund, Nature **440**, 297 (2006).
[55] E. Evans and K. Ritchie, Biophys. J. **76**, 2439 (1999).
[56] O. H. Willemsen, M. M. E. Snel, A. Cambi, J. Greve, B. G. D. Grooth, and C. G. Figdor, Biophys. J. **79**, 3267 (2000).
[57] C.-K. Lee, Y.-M. Wang, L.-S. Huang, and S. Lin, Micron **38**, 446 (2007).